Investigation of spatial structure and sympathetic cooling in the $^{9}Be^{+}$–$^{40}Ca^{+}$ bi-component Coulomb crystals

Min Li(李敏)[1,2], Yong Zhang(张勇)[1,2], Qian-Yu Zhang(张乾煜)[1,2], Wen-Li Bai(白文丽)[1,2], Sheng-Guo He(何胜国)[1], Wen-Cui Peng(彭文翠)[1,‡], and Xin Tong(童昕)[1,†]

[1] *State Key Laboratory of Magnetic Resonance and Atomic and Molecular Physics, Innovation Academy for Precision Measurement Science and Technology, Chinese Academy of Sciences, Wuhan* 430071, *China*

[2] *University of Chinese Academy of Sciences, Beijing* 100049, *China*

(Received 3 March 2022; revised manuscript received 8 May 2022; accepted manuscript online 18 May 2022)

We study the spatial structure and sympathetic cooling of the bi-component Coulomb crystal (CC), which consists of approximate 450 $^{9}Be^{+}$ ions and 450 $^{40}Ca^{+}$ ions with a mass ratio of 0.225 in a segmented linear ion trap. By two-dimensional imaging of the bi-component CC, the $^{9}Be^{+}$ ions are found to be surrounded by the $^{40}Ca^{+}$ ions in the radial direction with a separation ratio of ~ 2.0, and the axial length of the $^{9}Be^{+}$ ions occupied area is much larger than that of the $^{40}Ca^{+}$ ions occupied area. Combined with the previous experimental results, the structure of the $^{9}Be^{+}$–$^{40}Ca^{+}$ CC shows the larger the difference in the mass–charge ratio, the larger the separation between the two species. The comparison of the fluorescence spectra of the $^{9}Be^{+}$ ions in the bi-component CC and the pure CC indicates that the $^{9}Be^{+}$ ions can be sympathetically cooled and stably localized by the laser-cooled $^{40}Ca^{+}$ ions during the recording of the fluorescence spectrum.

Keywords: Coulomb crystals, sympathetic cooling, fluorescence spectrum

PACS: 64.70.kp, 37.10.Rs, 33.50.Dq **DOI:** 10.1088/1674-1056/ac70b2

1. Introduction

Laser cooling of the trapped ions to ultralow temperatures has made significant progress in various applications, including quantum computing,[1] quantum information,[2] optical clocks,[3,4] and high accuracy spectroscopy.[5] For direct laser cooling, however, a closed optical cycling transition between the energy levels is necessary and the transition frequencies are required to be accessible for available lasers.[6] Thus, there exist only a few species of ions that can be directly laser cooled. On the other hand, sympathetic cooling by using the Coulomb interactions between the laser-cooled (LC) ions and the sympathetically cooled (SC) ions can overcome this limitation. It allows more ionic species of the atoms and molecules to be cooled down to ultralow temperatures, keeps the ions in a stable Coulomb crystal (CC) structure, and prolongs the trapping time of the ions. For example, in the determination of the fundamental constants research, molecular hydrogen ions are sympathetically cooled by the laser-cooled $^{9}Be^{+}$ ions forming a bi-component CC, and their rovibrational spectroscopy is measured with tens of ppt accuracy.[7,8] In the field of low-temperature chemistry, the bi-component CC also enables the studies of ultracold chemical reactions at the milli-Kelvin level.[9] Furthermore, for fundamental physics tests, positrons at an ultralow temperature have been successfully prepared by the laser-cooled $^{9}Be^{+}$ ions,[10,11] and antiprotons at an ultralow temperature are also proposed to be prepared by the laser-cooled Th^{-} anions through sympathetic cooling.[12]

In a bi-component CC, the Coulomb interaction between the SC ions and the LC ions strongly depends on the structures of the CC and the distances between the components.[13] Illuminating the ions of the two species in a linear ion trap simultaneously can give a clear image of the bi-component CC structure and derive the spatial separation, which is closely related to the mass ratio between the different components with the same charge. In 2001, Drewsen's group illuminated the bi-component crystal of $^{24}Mg^{+}$–$^{40}Ca^{+}$ with a mass ratio of 0.6 and derived the corresponding radial separation ratio of ~ 0.78 in their experiment.[14] Later, they observed and analyzed the three-dimensional structures of the $^{40}Ca^{+}$ component in a bi-component CC of $^{40}Ca^{+}$–$^{44}Ca^{+}$ ions with a mass ratio of 0.91 in 2007.[15] In 2019, the group of Wang prepared a bi-component CC of $^{24}Mg^{+}$–$^{113}Cd^{+}$ with a mass ratio of 0.21 for the study of the microwave frequency standard and observed the spatial separation between $^{24}Mg^{+}$ and $^{113}Cd^{+}$. Recently, they also obtained the bi-component CC of $^{40}Ca^{+}$–$^{113}Cd^{+}$ with a mass ratio of 0.35 and estimated the radial separation ratio of ~ 0.59 combining with the theoretical zero-temperature charged-liquid model.[16–18]

In this work, the bi-component CC of $^{9}Be^{+}$–$^{40}Ca^{+}$ with a mass ratio of 0.225 is prepared in a segmented linear ion trap, and the radial separation and the axial distribution are investigated by the simultaneous imaging of both species. To study the sympathetic cooling efficiency of $^{40}Ca^{+}$ ions on

†Corresponding author. E-mail: tongxin@wipm.ac.cn
‡Corresponding author. E-mail: wencuipeng@wipm.ac.cn

© 2023 Chinese Physical Society and IOP Publishing Ltd

$^{9}Be^{+}$ ions, the fluorescence spectra and ionic crystal images of the $^{9}Be^{+}$ ions with the changing of the 313 nm laser detuning in a bi-component CC are compared with those in a pure $^{9}Be^{+}$ CC.

2. Experimental setup

The experimental setup is shown in Fig. 1, the segmented linear ion trap has been described in detail in our previous work[19] and the trapping parameters a and q for the two ion species are set as $q_{Ca} \approx 0.02$, $q_{Be} \approx 0.09$, $a_{Ca} \approx 0$, and $a_{Be} \approx 0$ to trap $^{40}Ca^{+}$ and $^{9}Be^{+}$ simultaneously. The $^{40}Ca^{+}$ ions are firstly loaded into the ion trap by photoionizing the neutral atoms from a Ca oven.[20] The laser cooling of the $^{40}Ca^{+}$ ions is achieved by a cooling laser of 397 nm on the transition of $4s\ ^{2}S_{1/2} \leftrightarrow 4p\ ^{2}P_{1/2}$ and a repumping laser of 866 nm on the transition of $3d\ ^{2}D_{3/2} \leftrightarrow 4p\ ^{2}P_{1/2}$ as illustrated in Fig. 2(a). Once the 397 nm and 866 nm lasers are tuned to proper frequencies, the $^{40}Ca^{+}$ ions are efficiently laser cooled and form a pure ultracold CC.[21] The $^{9}Be^{+}$ ions are then loaded into the ion trap by photoionizing the atomic Be beam produced by a Be oven.[22] The trapped $^{9}Be^{+}$ ions are sympathetically cooled by the ultracold $^{40}Ca^{+}$ ions to form a $^{9}Be^{+}$–$^{40}Ca^{+}$ bi-component CC. The $^{9}Be^{+}$ ions appear as a dark core in the center area of the bi-component CC if the 313 nm laser is not introduced or at large detuning from the $^{9}Be^{+}$ resonance.

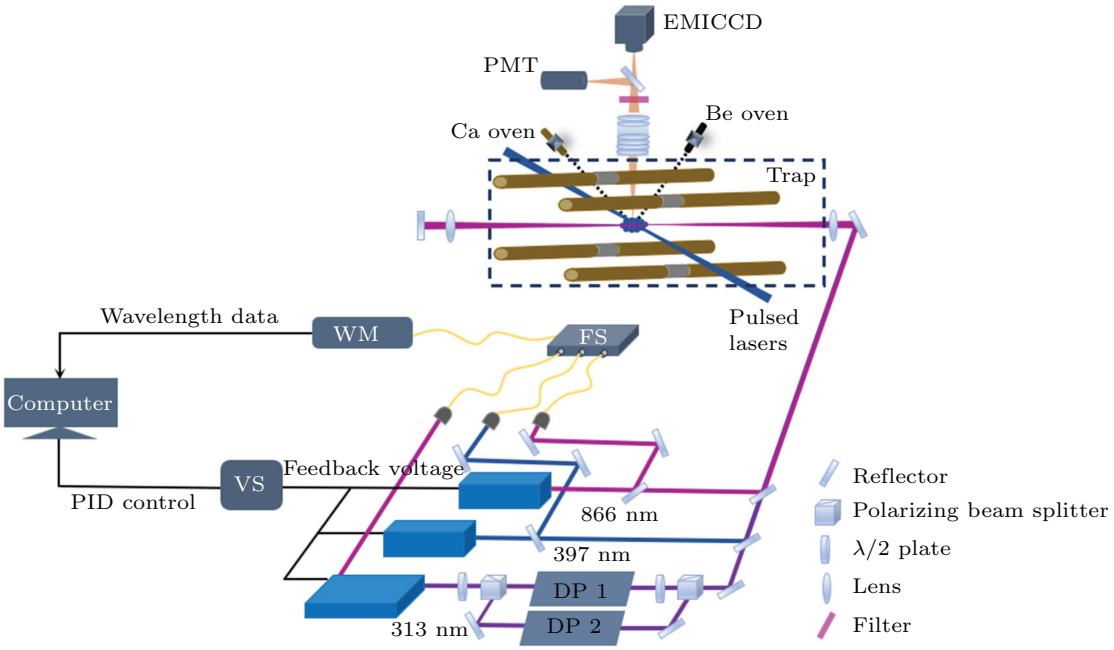


Fig. 1. Schematic of the experiment setup, including an ion trap, the lasers with frequency locking syste, and the fluorescence collecting system. FS: fiber switch, WM: wavelength meter, VS: voltage source, DP: double pass.

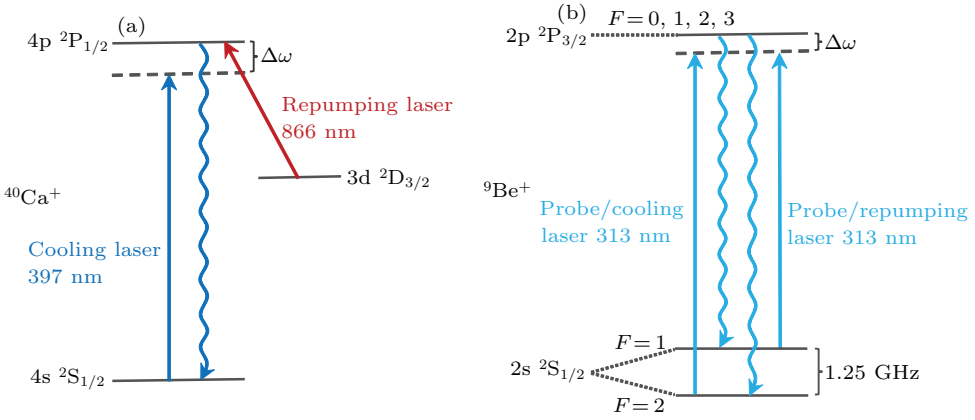


Fig. 2. Relevant energy levels of Doppler laser-cooling for $^{40}Ca^{+}$ (a) and detection or laser-cooling for $^{9}Be^{+}$ (b), respectively.

The $^{9}Be^{+}$ ions can also be directly laser cooled by a 313 nm laser along the trap axis on the transition of $2s\ ^{2}S_{1/2} \leftrightarrow 2p\ ^{2}P_{3/2}$ as shown in Fig. 2(b). A double pass scheme is used to couple the two hyperfine levels of $2s\ ^{2}S_{1/2}$ state with 1.25 GHz splitting. The cooling and repumping laser beams work as probe beams for simplicity. The frequency stabilization of all lasers can be realized by the computer control with a precision wavelength meter (HighFinesse WSU/10) cal-

ibrated by a helium–neon laser (Thorlabs HRS015B). The fluorescence of the $^{40}Ca^+$ and $^{9}Be^+$ ions is recorded by a photomultiplier tube (PMT, Hamamatsu Photonics R1464) and imaged onto an electron-multiplying intensified CCD camera (EMICCD, Princeton Instruments MAX 4-512EM(B)) by a magnification lens system simultaneously. Due to the chromatic aberration, the correction of focus positions is required for imaging of $^{9}Be^+$ and $^{40}Ca^+$ ions separately by means of color filters. By combining the images of the two ion species, the synthetic image of the bi-component CC is obtained. During the detection of the $^{9}Be^+$ ions, the frequencies of 397 nm and 866 nm lasers are stabilized to ensure the ultralow temperature of the $^{40}Ca^+$ ions CC.

2.1. Equations of motion and forces for the ions in the linear ion trap

After a bi-component CC is prepared, the ions in the crystal are in a dynamic equilibrium, and the classical equation of motion for the LC ions can be expressed in a general term as[13,23]

$$M_i \frac{\mathrm{d}\boldsymbol{r}^2}{\mathrm{d}^2 t} = \boldsymbol{F}_i^{\mathrm{Coulomb}} + \boldsymbol{F}_i^{\mathrm{trap}} + \boldsymbol{F}_i^{\mathrm{laser}} + \boldsymbol{F}_i^{\mathrm{random}}. \tag{1}$$

It includes the Coulomb force $\boldsymbol{F}_i^{\mathrm{Coulomb}}$, the trapping force $\boldsymbol{F}_i^{\mathrm{trap}}$, the laser force $\boldsymbol{F}_i^{\mathrm{laser}}$, and the stochastic force $\boldsymbol{F}_i^{\mathrm{random}}$. In the case of the SC ions, the expression of the forces is the same as that of the LC ions, except that the laser force $\boldsymbol{F}_i^{\mathrm{laser}} = 0$. The Coulomb force $\boldsymbol{F}_i^{\mathrm{Coulomb}}$ is the Coulomb repulsive forces between the i-th ion and all other ions in the trap, described as

$$\boldsymbol{F}_i^{\mathrm{Coulomb}} = \frac{Q_i}{4\pi\varepsilon_0} \nabla \sum_{j=1, j\neq i}^{j=N} \frac{Q_j \boldsymbol{r}_{ij}}{\left|\boldsymbol{r}_{ij}\right|^2}, \tag{2}$$

where ε_0 is the vacuum permittivity, Q is the charge of the ion, and $\boldsymbol{r}_{ij}$ is the vector of the distance between the i-th and the j-th ions.

The trapping force $\boldsymbol{F}_i^{\mathrm{trap}}$ is the combination of the radial $\boldsymbol{F}_{\mathrm{radial}}$ and axial $\boldsymbol{F}_{\mathrm{axial}}$ trapping forces which can be derived as[24,25]

$$\boldsymbol{F}_{\mathrm{radial}} = -\left(\frac{\kappa_r^2 Q^2 U_{\mathrm{rf}}^2 r}{2M r_0^4 \Omega_{\mathrm{rf}}^2} - \frac{\kappa_z Q U_{\mathrm{end}} \boldsymbol{r}}{z_0^2}\right), \tag{3}$$

$$\boldsymbol{F}_{\mathrm{axial}} = -\frac{2\kappa_z Q U_{\mathrm{end}} \boldsymbol{z}}{z_0^2}, \tag{4}$$

where U_{rf} is the amplitude of the RF trapping field at the frequency of Ω_{rf}, $2r_0$ is the distance between two diagonal electrodes, M is the mass of the trapped ions, U_{end} is the endcap voltage, $2z_0$ is the distance between the end-caps of the linear Paul trap, and κ_r and κ_z are the geometry parameters of the trap in the radial and axial directions, respectively. F_{radial} is proportional to the distance $\boldsymbol{r}$ from the central axis of the trap and inversely proportional to the mass of the trapped ions. This results in that in the bi-component CC, the heavier ions are confined radially weaker than the lighter ones.

3. Experimental results

3.1. The spatial structure of the bi-component Coulomb crystals

The image of a $^{9}Be^+$–$^{40}Ca^+$ bi-component CC containing approximately 450 $^{9}Be^+$ ions and 450 $^{40}Ca^+$ ions is shown in Fig. 3, under the trapping condition of $U_{\mathrm{rf}} = 304$ V at $\Omega_{\mathrm{rf}} = 2\pi \times 11.8$ MHz and $U_{\mathrm{end}} = 0.7$ V. The lasers for cooling $^{40}Ca^+$ ions (397 nm and 866 nm) and detecting $^{9}Be^+$ ions (313 nm) are stabilized to frequencies where the $^{40}Ca^+$ are efficiently laser cooled and the $^{9}Be^+$ ions are clearly detected. The temperature of the ions is about 10 mK where an ordered structure of the bi-component CC is shown and the individual ions can be observed.[26,27] In the radial direction, the $^{9}Be^+$ ions are radially surrounded by the $^{40}Ca^+$ ions, the radial separation $r_{Ca^+} - r_{Be^+}$ is about 50 μm, where r_{Ca^+} is the inner radius of the $^{40}Ca^+$ shell and r_{Be^+} is the outer radius of the $^{9}Be^+$ core. The radial separation is caused by the different radial trapping force according to Eq. (3), and the $^{9}Be^+$ ions are confined radially more strongly than $^{40}Ca^+$ ions due to the lower mass. In the zero-temperature charged-liquid model,[28,29] the separation ratio of the two ion species is $r_{Ca^+}/r_{Be^+} = \sqrt{M_{Ca^+}/M_{Be^+}} = 2.1$, which agrees with our experiment result $r_{Ca^+}/r_{Be^+} \approx 2.0$. In the axial direction, the length of the distribution area of the $^{9}Be^+$ ions (~ 1250 μm) is much greater than the corresponding length of the $^{40}Ca^+$ ions (~ 760 μm). It is in line with the different aspect ratios ($L/R \sim 12.5$ for $^{9}Be^+$ and ~ 2.1 for $^{40}Ca^+$) for $^{9}Be^+$ and $^{40}Ca^+$ ions under the same trapping condition.[30,31] The reason for the large aspect ratio difference for the two ion species is that the axial potentials are the same for both species, whereas the radial potentials are mass-dependent.

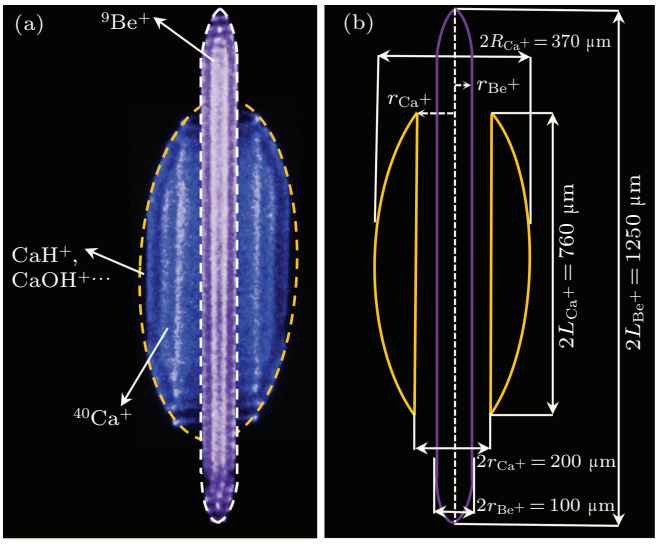


Fig. 3. (a) The synthetic EMICCD image of a $^{9}Be^+$–$^{40}Ca^+$ bi-component CC by combining the separately recorded fluorescence images of $^{9}Be^+$ and $^{40}Ca^+$ ions. The yellow dashed line represents the fitting boundaries of the $^{40}Ca^+$ ions with a few dark ions caused by chemical reactions, and the white dashed line shows the fitting boundaries of the $^{9}Be^+$ ions. (b) Fitting dimensions of the $^{9}Be^+$ and $^{40}Ca^+$ bi-component CC.

Combined with the different bi-component CCs in the previous experiments,[14,18] the $^{9}Be^{+}$–$^{40}Ca^{+}$ bi-component CC shows that the larger spatial separation of the two ion species in the radial direction, and the larger distribution difference in the axial direction. As the Coulomb interaction is inversely proportional to the square of the distance,[13] the sympathetic cooling effect between the two ion species with a larger mass–charge difference is also weaker. For effective sympathetic cooling, therefore, it is necessary to choose the proper LC ions to reduce the difference in the mass–charge ratio of the two ion species.

3.2. The comparison of the fluorescence spectra and ionic crystal images of the $^{9}Be^{+}$ ions in the bi-component CC and the pure CC

To study the sympathetic cooling efficiency, the intensities of the $^{9}Be^{+}$ fluorescence signal (the sampling time is 200 ms) are measured as a function of the 313 nm laser frequency detuning of the transition 2s $^{2}S_{1/2}$ ($F = 1, 2$) $\leftrightarrow$ 2p $^{2}P_{3/2}$ in both the pure and bi-component CCs as illustrated in Fig. 4(a). The frequency of the 313 nm laser is scanned with a rate of 3 MHz/s around the resonant frequency ($\Delta\omega =$ 0 MHz) over a range of 1.6 GHz. The frequency detuning $\Delta\omega = -400$ MHz, -150 MHz, -100 MHz, 0 MHz, 110 MHz, and 400 MHz are denoted in turn as the set-points from 1 to 6, where the corresponding images of the pure $^{9}Be^{+}$ ions and the $^{9}Be^{+}$–$^{40}Ca^{+}$ bi-component ions are also separately recorded as Figs. 4(b)6 and 4(c)6, respectively.

The spectrum of the pure $^{9}Be^{+}$ ions below 0 MHz detuning (red detuning) is almost as same as that of the $^{9}Be^{+}$ ions in bi-component CC as shown in Fig. 4(a). The maximum fluorescence signals of both crystals are at the set-point 3 ($\Delta\omega = -100$ MHz) and about ten times larger than the background signals (e.g., at the set-points 1 and 6). When the frequency of the 313 nm laser is detuned from the 0 MHz offset (set-point 4) to a blue offset frequency, the intensity of the fluorescence of the pure $^{9}Be^{+}$ ions drops rapidly and almost vanishes at the set-point 5 ($\Delta\omega = 110$ MHz). However, in the bi-component CC, the fluorescence signal of the $^{9}Be^{+}$ ions keeps at a high level from the set-point 4 ($\Delta\omega = 0$ MHz) to the set-point 5 ($\Delta\omega = 110$ MHz).

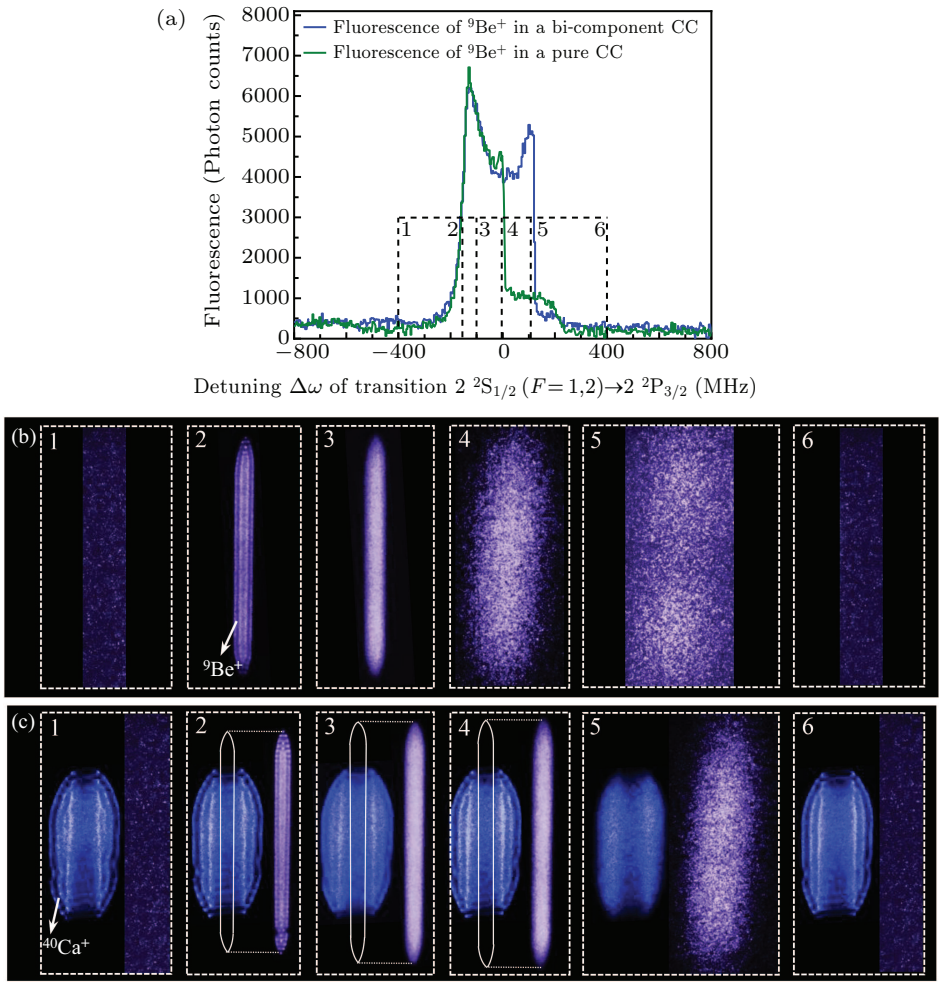


Fig. 4. The fluorescence signal of $^{9}Be^{+}$ ions and $^{40}Ca^{+}$ ions changes with the frequency detuning of the 313 nm detection laser. The spectra of pure $^{9}Be^{+}$ ions (green) and bi-component $^{9}Be^{+}$ ions (blue) are shown in (a). At the detuning $\Delta\omega = -400$ MHz, -150 MHz, -100 MHz, 0 MHz, 110 MHz, 400 MHz denoted in turn as the set-points of 1 to 6, the images of the pure $^{9}Be^{+}$ ions and the $^{9}Be^{+}$–$^{40}Ca^{+}$ bi-component ions are illustrated in (b) and (c), respectively.

Similar to the fluorescence spectra, the images of the $^{9}Be^{+}$ ions in both bi-component and pure CCs are generally no different at the red detuned range of the 313 nm laser as shown in Figs. 4(b)3 and 4(c)3. In both the pure and bi-component CCs, one can also see that the $^{9}Be^{+}$ ions form a clear ordered structure at the set-point 2, while the blurred image at the set-point 3 indicates the slightly increased temperature of the $^{9}Be^{+}$ ions due to the insufficient cooling force at the small red detuning of the 313 nm laser.

The significant difference between the images of the $^{9}Be^{+}$ ions in the pure and bi-component CCs appears at the set-points of 4 and 5, where the 313 nm laser is blue detuning. At the set-point 4, the ions in the pure $^{9}Be^{+}$ CC are delocalized as the ionic cloud, while the $^{9}Be^{+}$ ions in the bi-component CC remain their crystal state. At the detuning of 110 MHz, the pure $^{9}Be^{+}$ ions fill the whole trapping volume in the ion trap as shown in Fig. 4(b)5, while the $^{9}Be^{+}$ ions in the bi-component CC are sympathetically cooled by the LC $^{40}Ca^{+}$ ions and remain as the tight ionic cloud. The $^{40}Ca^{+}$ ions are also heated to a blurred ionic cloud state by the $^{9}Be^{+}$ ions which are heated by the blue detuned 313 nm laser at the set-point 5. At the detuning of 400 MHz, the fluorescence signal vanishes in both the pure and bi-component CCs as shown in Fig. 4(a), however, the $^{9}Be^{+}$ ions remain localized in the bi-component CC as a dark core due to the dominating sympathetic cooling force from the LC $^{40}Ca^{+}$ ions.

The results from Fig. 4 indicate that although the Doppler laser cooling is ineffective when the 313 nm laser is at the blue detuned range, the $^{9}Be^{+}$ ions can be cooled by the laser-cooled $^{40}Ca^{+}$ ions through sympathetic cooling. While in the red detuned range, the existing laser cooling force is much stronger than the sympathetic cooling force and dominates the cooling process.

4. Conclusion and outlook

In conclusion, the $^{9}Be^{+}$ ions are sympathetically cooled by the $^{40}Ca^{+}$ ions and detected by the 313 nm laser, the spatial structure of the bi-component CC and the sympathetic cooling effect are directly observed in a segmented linear ion trap. In the $^{9}Be^{+}$–$^{40}Ca^{+}$ bi-component CC, the mass ratio of 0.225 between SC and LC ions is lower than the bound ratio of 0.54, which is obtained by a priori molecular dynamical calculation combining with a heat-exchange model of sympathetic cooling.[32] Combined with the bi-component CCs in the previous experiments, the $^{9}Be^{+}$–$^{40}Ca^{+}$ bi-component CC shows that the larger the difference in the mass–charge ratio leads to the larger the spatial separation between the two ion species.[14–18] Comparing the fluorescence of the $^{9}Be^{+}$ ions in the pure and bi-component CCs with the changing of the laser detuning, it found that although the sympathetic cooling force is much weaker than the laser cooling force, it can still help the $^{9}Be^{+}$ ions remain ultracold and localized inside the ion trap. We expect that this work will benefit the determination of the number of dark ions in the bi-component CC with a large difference in the mass–charge ratio, such as the Be^{+}–H_2^{+} and Be^{+}–HD^{+},[33,34] and it may further improve the accuracy of the rovibrational spectroscopy of H_2^{+} or HD^{+}.[35]

Acknowledgements

Project supported by the National Natural Science Foundation of China (Grant No. 91636216), and the Strategic Priority Research Program of the Chinese Academy of Sciences (Grant No. XDB21020200).

References

[1] Johri S, Debnath S, Mocherla A, Singk A, Prakash A, Kim J and Kerenidis I 2021 *Npj. Quantum. Inform* **7** 122
[2] Hannegan J, Siverns J D, Cassell J and Quraishi Q 2021 *Phys. Rev. A* **103** 052433
[3] Brewer S M, Chen J S, Hankin A M, Clements E R, Chou C W, Wineland D J, Hume D B and Leibrandt D R 2019 *Phys. Rev. Lett.* **123** 033201
[4] Zhang Q X, Wang Y R, Zhu C H, Wang Y X, Zhang X, Gao K Y and Zhang W 2020 *Chin. Phys. B* **29** 093203
[5] Micke P, Leopold T, King S A, Benkler E, Spieß L J, Schmöger L, Schwarz M, Crespo López-Urrutia J R and Schmidt P O 2020 *Nature* **578** 60
[6] Chu S, Hollberg L, Bjorkholm J E, Cable A and Ashkin A 1985 *Phys. Rev. Lett.* **55** 48
[7] Patra S, Germann M, Karr J Ph, Haidar M, Hilico L, Korobov V I, Cozijn F M J, Eikema K S E, Ubachs W and Koelemeij J C J 2020 *Science* **369** 1238
[8] Alighanbari S, Giri G S, Constantin F L, Korobov V I and Schiller S 2020 *Nature* **581** 152
[9] Willitsch S, Bell M T, Gingell A D and Softley T P 2008 *Phys. Chem. Chem. Phys.* **10** 7200
[10] Baker C J, Bertsche W, Capra A, *et al.* 2021 *Nat. Commun.* **12** 6139
[11] Jelenković B M, Newbury A S, Bollinger J J, Itano W M and Mitchell T B 2003 *Phys. Rev. A* **67** 063406
[12] Tang R L, Si R, Fei Z J, Fu X X, Lu Y Z, Brage T, Liu H T, Chen C Y and Ning C G 2021 *Phys. Rev. A* **103** 042817
[13] Zhang C B, Offenberg D, Roth B, Wilson M A and Schiller S 2007 *Phys. Rev. A* **76** 012719
[14] Hornekær L, Kjærgaard N, Thommesen A M and Drewsen M 2001 *Phys. Rev. Lett.* **86** 1994
[15] Mortensen A, Nielsen E, Matthey T and Drewsen M 2007 *J. Phys. B: At. Mol. Opt. Phys.* **40** 223
[16] Han J Z, Qin H R, Xin N C, Yu Y M, Dzuba V A, Zhang J W and Wang L J 2021 *Appl. Phys. Lett.* **118** 101103
[17] Miao S N, Qin H R, Xin N C, Chen Y T, Zhang J W and Wang L J 2022 comarXiv:2201.03377v1 [physics.atom-ph]
[18] Zuo Y N, Han J Z, Zhang J W and Wang L J 2019 *Appl. Phys. Lett.* **115** 061103
[19] Li H X, Zhang Y, He S G and Tong X 2019 *Chin. J. Phys.* **60** 61
[20] Li H X, Li M, Zhang Q Y and Tong X 2019 *Chin. Phys. Lett.* **36** 073701
[21] Du L J, Chen T, Song H F, Chen S L, Li H X, Huang Y, Tong X, Gao K L and Guan H 2015 *Chin. Phys. B* **24** 083702
[22] Li M, Zhang Y, Zhang Q Y, Bai W L, He S G, Peng W C and Tong X 2022 *J. Phys. B: At. Mol. Opt. Phys.* **55** 035002

[23] Du L J, Song H F, Li H X, Chen S L, Chen T, Sun H Y, Huang Y, Tong X, Guan H and Gao K L 2015 *Chin. Phys. B* **24** 113703
[24] Dehmelt H 1967 *Radiofrequency spectroscopy of stored ions. I: Storage* (Seattle: University of Washington) pp. 53–72
[25] Du L J 2015 *Research on dynamics of ion crystal in a linear radio-frequency trap* (Ph.D Dissertation) (Wuhan: Chinese Academy of Sciences (in Chinese) pp. 36–40
[26] Tong X, Winney A H and Willitsch S 2010 *Phys. Rev. Lett.* **105** 143001
[27] Slattery W L, Doolen G D and DeWitt H E 1980 *Phys. Rev. A* **21** 2087
[28] Wineland D J 1987 *Proceedings of the Cooling, Condensation and Storage of Hydrogen Cluster Ions Workshop "Ion Traps for Large Storage Capacity"*, June 30–July 11, 1986, State of California, American, p. 181
[29] Hornekær L 2000 *Single-and multi-species Coulomb ion crystals: Structures, dynamics and sympathetic cooling* (Ph. D. Dissertation) (Denmark: University of Aarhus) (in English) pp. 106–113
[30] Turner L 1987 *Phys. Fluids* **30** 3196
[31] Kjaergaard N and Drewsen M 2003 *Phys. Rev. Lett.* **91** 095002
[32] Baba T and Waki I2002 *Appl. Phys. B* **74** 375
[33] Alighanbari S, Hansen M G, Korobov V I and Schiller S 2018 *Nat. Phys.* **14** 555
[34] Schmidt J, Louvradoux T, Heinrich J, Sillitoe N, Simpson M, Karr J P and Hilico L 2020 *Phys. Rev. Appl.* **14** 024053
[35] Zhong Z X, Tong X, Yan Z C and Shi T Y 2015 *Chin. Phys. B* **24** 053102